

Exciton broadening in WS₂/graphene heterostructures

Heather M. Hill,^{1,2} Albert F. Rigosi,^{1,2} Archana Raja,^{1,2} Alexey Chernikov,^{1,3} Cyrielle Roquelet,^{1,4} and Tony F. Heinz^{1,2}

¹*Departments of Physics, Electrical Engineering, and Chemistry, Columbia University, New York, New York 10027, USA*

²*Department of Applied Physics, Stanford University, Stanford, California 94305, USA*

and SLAC National Accelerator Laboratory, 2575 Sand Hill Road, Menlo Park, California 94025, USA

³*Department of Physics, University of Regensburg, Regensburg 93053, Germany*

⁴*ArcelorMittal Maizières Research SA, Maizières-lès-Metz 57280, France*

(Received 17 August 2017; revised manuscript received 16 September 2017; published 1 November 2017)

We have used optical spectroscopy to observe spectral broadening of WS₂ exciton reflectance peaks in heterostructures of monolayer WS₂ capped with mono- to few-layer graphene. The broadening is found to be similar for the A and B excitons and on the order of 5–10 meV. No strong dependence on the number of graphene layers was observed within experimental uncertainty. The broadening can be attributed to charge- and energy-transfer processes between the two materials, providing an observed lower bound for the corresponding time scales of 65 fs.

DOI: [10.1103/PhysRevB.96.205401](https://doi.org/10.1103/PhysRevB.96.205401)

I. INTRODUCTION

Due to its unique electronic and optical properties [1–4], graphene is a promising material for use in optoelectronics and photovoltaics. The extensive study of graphene has led to the investigation of the semiconducting transition-metal dichalcogenide semiconductors (TMDCs), which exhibit direct gaps as monolayers [5–9], strong light emission and absorption in the visible range [10–15], coupled valley and spin degrees of freedom [16–25], and large exciton and trion binding energies [26–35]. Combinations of TMDC layers and graphene have already been assembled into heterostructures [36], photodetectors [37], multifunctional photoresponsive memory devices [38], and vertical field effect transistors [39]. Much recent effort has been focused on interlayer interactions in TMDC heterostructures [40–52]. Specifically, charge-transfer processes have been invoked to explain line broadening observed in the excitonic features in TMDC/TMDC heterostructures compared to the corresponding linewidth in the isolated monolayers [51]. The broadening effects, as well as narrowing effects that may arise from reduced static charging and the screening of inhomogeneous potentials from the substrate, as seen in TMDC/hexagonal boron nitride (h-BN) heterostructures [53], are expected to play a role in the case of TMDC/graphene heterostructures. Such TMDC/graphene structures have been introduced for various device applications and have also been of particular interest in the spectroscopy community [54–57]. In a recent report, we examined the influence of graphene on renormalization of the TMDC band gap due to dielectric screening in graphene-covered TMDC samples [58], determined spectroscopically through characterization of the fundamental Rydberg exciton series.

In this paper, we examine changes in the linewidth of excitons in the TMDC monolayers caused by the presence of an adjoining graphene layer in a vertical heterostructure. Through careful absorption measurements of the A and B excitons in monolayer WS₂, we identify exciton line broadening of at least 5 meV induced by mono- and few-layer graphene. We discuss the possible mechanisms responsible for this observation, particularly the impact of the fundamental processes of energy and charge transfer from the semiconducting WS₂ to graphene.

Our study provides an upper bound on the observed rate of these processes and, hence, a lower limit for the energy- and charge-transfer times extracted from the observed broadening. These results also complement the recent time-resolved pump-probe studies of TMDC/graphene heterostructures [59].

II. EXPERIMENTAL METHODS

A. Sample preparation

The monolayer WS₂ samples were prepared by exfoliating bulk crystal onto fused silica substrates. We verified the layer thickness using photoluminescence (PL) and Raman spectroscopy. Subsequently, graphene was exfoliated on polypropylene carbonate (PPC) that was spin-cast on a silicon wafer. The thickness of the exfoliated graphene was confirmed with Raman spectroscopy and reflectance contrast measurements. We found mono-, bi-, tri-, and tetralayer graphene flakes. The selected graphene layers were then transferred onto monolayer WS₂ flakes following the procedure described in the Supplemental Material of Ref. [51]. The residual PPC was removed with acetone followed by an isopropanol rinse. The samples were not annealed to prevent any modification to their optical properties. To facilitate spectroscopic comparison, the structure was prepared so that there were accessible regions of uncovered, pristine WS₂ in addition to the WS₂/graphene heterostructure.

B. Reflectance contrast measurements

We obtained information about the optical absorption of the sample by measuring the reflectance spectrum from the sample on the substrate, R_s , as well the corresponding spectrum for the bare substrate, R_0 . We then constructed the reflectance contrast spectrum as $\Delta R/R = (R_s - R_0)/R_0$. For a thin sample with low absorption on a transparent substrate, as in our measurements, this reflectance contrast spectrum is approximately proportional to the absorption of the sample [6]. The reflectance measurements were performed using a tungsten-halogen lamp light source focused on the sample at normal incidence with a spot size of 2 μm . The reflected light was collected by a spectrometer equipped with a CCD cooled

by liquid nitrogen (LN). Most of our measurements were conducted at room temperature, but some were performed in a cryostat at 70 K cooled with LN. Measurements showing the extent of PL quenching and its relation to the observed exciton line broadening are provided in Sec. 5 of the Supplemental Material [60].

For each of the samples, the reflectance contrast spectrum was measured in three different regions: on bare WS₂ without graphene above it (both before and after heterostructure processing), on graphene on fused silica without WS₂ below it, and on the graphene/WS₂ heterostructure. The variation in exciton linewidth from measurements at several different points on the WS₂ samples was found to be less than 0.5 meV. This result indicates that the inhomogeneity of the sample was minor. We also determined that the linewidth of the WS₂ exciton in the isolated region of the material did not change more than 0.5 meV during the processing (i.e., mechanical transfer) required to prepare the heterostructure. See Sec. 7 of the Supplemental Material for more details [60].

III. EXPERIMENTAL RESULTS

Figure 1 shows the room temperature reflectance contrast spectra for a heterostructure composed of monolayer WS₂ and bilayer graphene. For the heterostructure, an expected increase in the reflection contrast occurs due to the broad

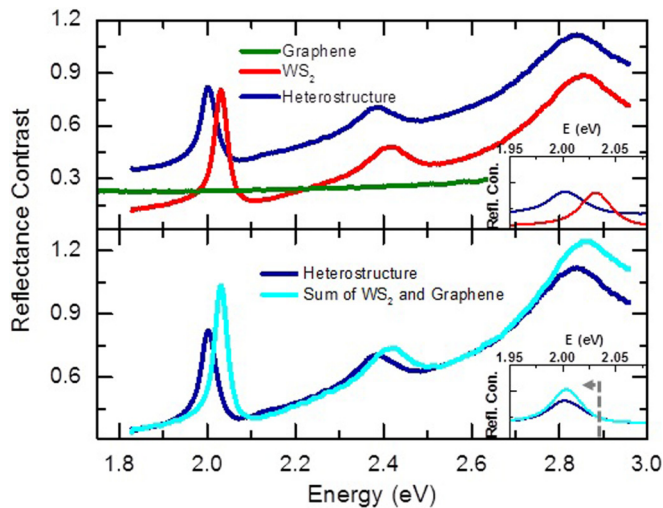


FIG. 1. (Top) The room temperature reflectance contrast spectrum of monolayer (1L) WS₂, 2L graphene, and WS₂/graphene heterostructure are shown. The red curve is the reflectance contrast of WS₂ on fused silica without graphene and the green line is the reflectance contrast of bilayer graphene on fused silica. The blue is the WS₂/graphene heterostructure. The inset presents an expanded view in of the A exciton. (Bottom) A comparison is made between the reflectance contrast of the heterostructure and the sum of the spectra of the constituent layers. The blue curve is the experimental reflectance contrast data from the heterostructure (as in the top half of the figure). The cyan curve is obtained by adding the graphene reflectance contrast spectrum to that of the bare WS₂ monolayer. The inset shows the A exciton features for both curves, with the summed curve redshifted by 23 meV to allow for a direct comparison of the line shapes.

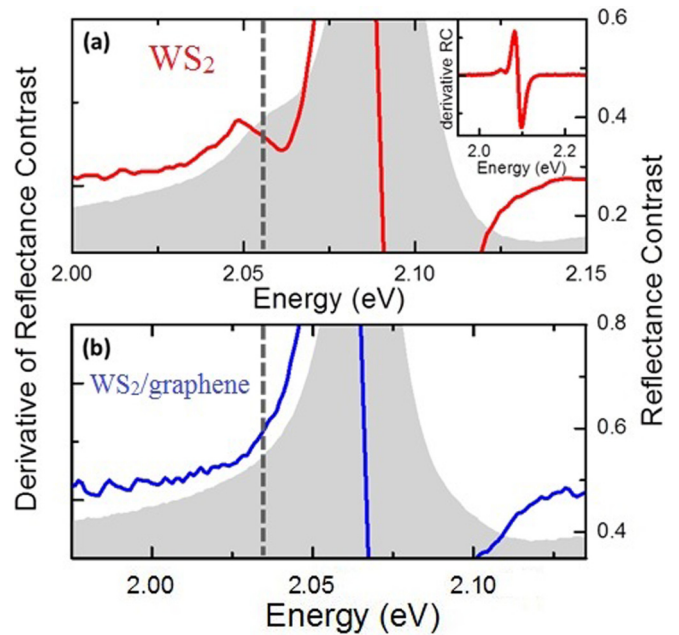


FIG. 2. Trion feature of the A exciton in the reflectance contrast spectrum of bare WS₂ and of the WS₂/graphene heterostructure, as measured at 70 K. (a) For bare WS₂, the (energy) derivative of the reflectance contrast spectrum is shown as a red line. The gray shading (right vertical scale) is the reflection contrast spectrum itself. The derivative of the reflectance contrast is plotted over a larger energy range in the inset. The position of the trion is indicated by a vertical dashed line. (b) The same data is plotted for a WS₂/graphene heterostructure. In this case, there is no signature of the trion absorption.

absorption of graphene. However, the heterostructure spectrum is not simply the sum of the isolated WS₂ and graphene absorption spectra. To demonstrate this, we plot in the bottom half of Fig. 1 the summed graphene and WS₂ spectrum compared to the measured heterostructure spectrum. We note two major differences: the measured exciton peaks in the heterostructure are broadened and redshifted. The bottom inset of Fig. 1 shows a redshifted, summed spectrum to allow a more direct comparison of the width of the A exciton peaks. We attribute the redshift to screening by the dielectric environment associated with the graphene. The relatively modest observed shift in the exciton transition energy reflects the combination of a significant renormalization of the quasiparticle band gap, offset by a decrease in the exciton binding energy [58].

In Fig. 2, we present reflectance contrast spectra for the sample at a temperature of approximately 70 K. In each panel we also show the spectrum's derivative, with respect to energy, to bring out weak features. As is typical for exfoliated samples on a substrate [27], a trion feature appears in the reflectance contrast of bare WS₂ due to unintentional doping of the sample. The corresponding peak position is about 2.05 eV, on the low-energy shoulder of the neutral A exciton. When WS₂ is capped with graphene, as shown in Fig. 2(b), the trion feature disappears. The absence of a trion feature for the WS₂/graphene heterostructure is not unexpected, since, upon contact, residual charges in the WS₂ could flow into lower-energy states via *static* charge transfer

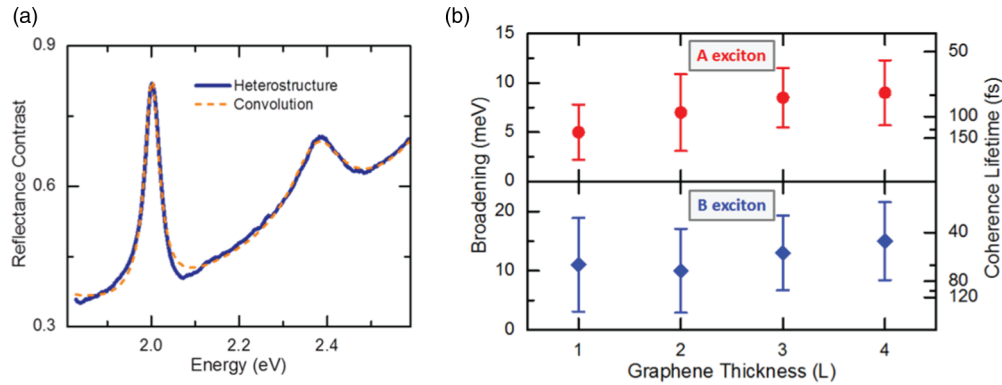


FIG. 3. (a) The room temperature reflectance contrast of a heterostructure is shown as well as the convolution of the sum of the individually measured constituent layers' spectra with a Lorentzian profile. The blue curve is the experimental reflectance contrast data from the heterostructure shown in Fig. 1. The dashed orange curve comes from convoluting the sum of the graphene and bare WS₂ reflectance contrast with a Lorentzian profile of 7 meV. (b) Linewidth broadening and coherence lifetimes for the A and B exciton of WS₂ in the heterostructure are presented as a function of the thickness of the graphene; the data were taken at room temperature. The top and bottom halves of the graph show the broadening of the A and B exciton peaks in the reflectance contrast, respectively. The thickness of the graphene is given in terms of layer numbers (L). Coherence lifetimes are obtained from the relation $\tau = \hbar/\Delta\Gamma$, accompanied by error bars associated with the extracted broadening uncertainty. The experimental range of lifetimes extracted with convolutions is 65 fs–130 fs, compared with the 55 fs–100 fs lifetime range extracted with the individual Lorentzian peak fitting, which assumes an ideal system and thus provides an even lower, yet theoretical bound to the lifetimes.

in the semimetallic graphene layer, whose Fermi energy is located in the gap of the WS₂. The evidence of *static* charge transfer to graphene, coupled with the Raman spectroscopy data provided in Sec. 6 of the Supplemental Material [60], will assist us in our overall interpretation of the exciton broadening in the discussion section.

To analyze the exciton line broadening more precisely, we try to replicate the heterostructure experimental data by starting with summed and redshifted WS₂ and graphene spectra for the isolated layers and then convoluting this spectrum for noninteracting layers with a Lorentzian line shape. The width of the Lorentzian is separately optimized for the A and B exciton features. Alternatively, we can simply fit each exciton feature in the isolated WS₂ to a Lorentzian peak and compare this width to that obtained in a similar fashion for the heterostructure. The latter procedure gives a broadening several meV less than the former but assumes negligible inhomogeneous broadening in the fitting process. The convolution method does not require any particular assumptions with respect to the underlying peak structure and line shape, since the spectra include both minor features from excited exciton states, as well as the broad shoulder from higher energy resonances, such as the C feature.

In Fig. 3(a), we compare the experimental reflectance contrast spectrum of the A exciton of the heterostructure with the reflectance contrast spectrum for noninteracting layers (i.e., taking the sum of the measured spectra of bare WS₂ and bare graphene). The latter spectrum was then convoluted with a Lorentzian peak to simulate the broadening we observe in the heterostructure's experimental data. The Lorentzian width, given by $\Delta\Gamma$, in the convolution integral provides an upper bound for the observed increase in homogeneous linewidth. If this broadening arises from a new decay channel for WS₂ excitons due to the presence of graphene, we then have a lower bound for the observed lifetime of this process, given by $\tau = \hbar/\Delta\Gamma$.

The broadening values and associated lifetimes for the A and B exciton transitions are shown in Fig. 3(b) as a function of the thickness of the graphene that is placed on top of the WS₂. We see that, within experimental uncertainty, the broadening does not have a strong dependence on graphene thickness up to tetralayer graphene and ranges between 5 and 10 meV. Overall, the broadening is 4–5 times less than that seen in TMDC/TMDC heterostructures [42,51,61], which was attributed to interlayer (i.e., not *static*) charge transfer.

IV. DISCUSSION

A. Phonon broadening and doping

We now discuss possible physical mechanisms leading to the exciton line broadening in the WS₂/graphene heterostructure. Several possible mechanisms can be identified, including enhanced phonon broadening in the heterostructure, changes in doping, and scattering within or between layers, including charge transfer and energy-transfer processes. The mention of charge transfer in the following arguments is *not* a reference to the distinct *static* charges moving from WS₂ to graphene upon the layers making initial contact. We proceed to argue that the dominant processes to consider are indeed the latter two phenomena: energy and charge transfer of photoexcited carriers from WS₂ to graphene.

At room temperature, the A exciton peak in a typical exfoliated monolayer WS₂ has a width of about 40 (± 10) meV, as in our samples. As indicated by temperature-resolved measurements and theoretical modeling [62,63], about 20 meV of this linewidth primarily arises from exciton scattering with thermally activated phonons and a small contribution from the radiative recombination on the order of several meV. When the WS₂ flake is in contact with graphene, we could in principle expect to see increased phonon scattering from interaction of excitons in WS₂ with the phonons in the graphene layer. However, this additional scattering is

unlikely given the expected inefficiency of such a process due to the small extension of the exciton wave function in the out-of-plane direction. That is further supported by the observation of similar broadening of the exciton linewidth at low temperatures, where the exciton-phonon-scattering contribution already in the WS₂ layer is on the order of only a few meV [63]. While the width of the excitonic features changes quite dramatically (the 70-K temperature spectrum is available in the Supplemental Material [60]), the broadening does not change to within 1 meV. This also implies that the processes giving rise to the broadening do not strongly depend on the temperature, unlike what we would expect for an additional exciton-phonon scattering channel.

As previously discussed in Fig. 2, the trion feature, seen clearly in the low-energy shoulder of the A exciton in the WS₂ spectrum, has undergone a strong reduction in the heterostructure spectrum. The bare WS₂ spectrum indicates doping on the order of $3 \times 10^{12} \text{ cm}^{-2}$, as extracted from the trion-exciton separation energy [64], typical for exfoliated samples on substrates. The heterostructure spectrum, however, has no obvious trion feature, strongly suggesting that the doping conditions across the WS₂ sample in contact with graphene are close to charge neutrality due to the expected transfer of the *static* charge to graphene. A change in the initial doping of a sample can change the width of the excitonic features in the reflectance contrast. However, typically a reduction in the doping would cause the peaks to become narrower, as previously observed in WS₂ monolayers [64]. In this case, a dedoping of a maximum carrier density of $3 \times 10^{12} \text{ cm}^{-2}$ would correspond to a linewidth narrowing of about 3 meV, in contrast to the observed increase of the linewidth [64]. Therefore, the change in doping cannot be considered as the cause of the observed broadening and may even lead to an overall underestimation of the extracted values for the broadening by a few meV.

B. Intervalley scattering as a source of broadening

In our system, the arbitrary angle between the layers and the general reconfiguration of the WS₂ band structure in the heterostructure may introduce intervalley scattering within the WS₂ layer as another possible broadening mechanism which comes from two potential sources. The first source would be from changes to the band structure of WS₂ such that it exhibits an indirect band gap at the *Q* or Γ point. The second source would be from the potential overlap or hybridization of electronic states from WS₂ with those in graphene at various parts of the Brillouin zone (BZ), perhaps at the *K* point in the case of resonant tunneling.

In MoS₂, the difference between the valence-band energy of Γ and *K* in the unperturbed, direct gap case, is 0.1 eV for monolayer MoS₂, but there is a 0.3-eV maximum shift due to the presence of graphene [65]. In the case of WS₂/graphene heterostructures, the Γ -point maximum is 0.3 eV below that of the *K* point from angle-resolved photoemission spectroscopy (ARPES) [66]. MoS₂/graphene heterostructures have been reported to form an indirect gap at the Γ point (with a difference less than 0.2 eV with the *K* point) [36], but other literature suggests that MoS₂/graphene retains its direct band gap [66]. Therefore, if the graphene layer causes a similar change in the

WS₂, it is unlikely that WS₂ forms an indirect band gap. In the second case, ARPES measurements suggest that there is no significant overlap of electronic states at the *K*, *Q*, or Γ point between graphene and WS₂ [66–68]. We will revisit this second case in the charge-transfer discussion.

The remaining two significant processes to consider are charge and energy transfer. The fastest time scales for either charge transfer or energy transfer to occur in this system is on the order of 100 fs, as extracted from the experimental linewidth broadening. If we compare our system to other low-dimensional systems, we can approximate the contribution from nonradiative energy transfer via near-field dipole-dipole interactions. For example, the energy-transfer rate from nanoparticles and nanoplatelets to graphene has been reported to be around 1 ns, where the distance from the emitter to graphene is on the order of a few nanometers [69–71]. Federspiel *et al.* experimentally observed a d^{-3} dependence for the energy-transfer rate between two-dimensional (2D) CdSe nanoplatelets and graphene [72]. Hernández-Martínez *et al.* calculate a d^{-4} energy-transfer rate between general 2D-2D interfaces [73], though at short length scales, the scaling deviates from this form when taking into account the nonlocal effects for graphene that become prominent at distances below 1 nm [57,73]. Gaudreau *et al.* also predict a similar enhancement in rates as a function of the distance to graphene [74]. We use both of these distance dependencies to obtain a range of expected energy-transfer rates. The separation between the donor and acceptor in our system is 0.5 nm from atomic force microscopy measurements (see Supplemental Material [60]). If we scale the 1-ns rate mentioned above, we obtain an expected rate for our system of 3 ps to 0.2 ps or a broadening of 0.2 meV to 2 meV. Furthermore, the enhanced oscillator strength for WS₂ in Ref. [27] compared to the platelets should further increase the rate of energy transfer and resultant broadening of the exciton line [75]. It is therefore conceivable that energy transfer contributes to the observed exciton broadening.

Concerning charge transfer, reported rates fall into a similar range for rare-gas adlayers on metal surfaces and similar systems (10–100 fs) [76,77]. Recent literature reports charge-transfer rates of tens of femtoseconds in TMDC/TMDC heterostructures [51,62]. Based on the previous discussion about treating the WS₂/graphene heterostructures as having a direct band gap, one must question whether charge can transfer from the *K* point of WS₂ into graphene directly or if it requires a phonon-assisted process, which is set to occur for phonon energies as low as 84 meV, based on the alignment parameters in Ref. [59]. To elaborate, since the basic reciprocal lattice parameters in WS₂ and graphene are 1.33 \AA^{-1} and 1.69 \AA^{-1} , respectively, 0.36 \AA^{-1} is the absolute momentum difference between the two *K* points only in the case where both materials are aligned. In this zero-degree orientation, one can depict the two materials' dispersions, as in Fig. 4, to see that a phonon is required to impart at least 0.36 \AA^{-1} of additional momentum, which is equivalent to 84 meV assuming the effective mass of the charge is $0.16m_0$ [27], to transfer charge from WS₂ to graphene. Since various Raman modes exist in WS₂, such as the $E_{2g}^1(\Gamma)$ and $A_{1g}(\Gamma)$, with respective energies of approximately 44 and 52 meV and

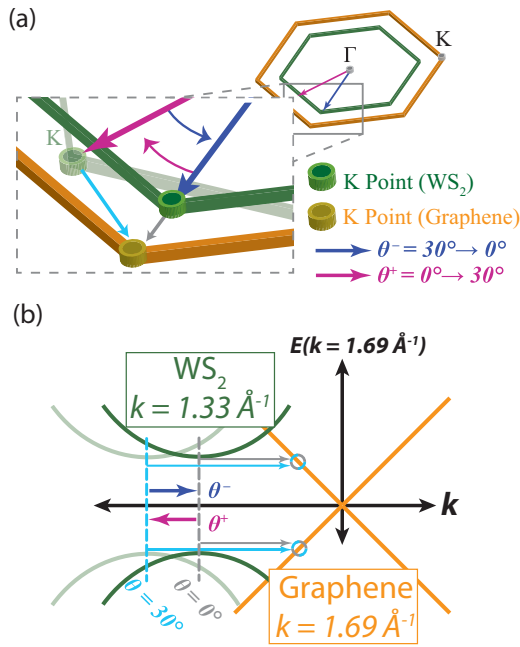


FIG. 4. A schematic is shown to elucidate the reason why resonant charge transfer is very unlikely as well as the concept of nonresonant charge transfer, a phenomenon likely to occur in the WS₂/graphene heterostructure. (a) The Brillouin zones of graphene (in orange) and WS₂ (in dark green) are depicted along with the K points in each. One corner of the zone is inspected more closely, showing that the relative orientation of the two zones can vary depending on the crystal orientations (which were arbitrary when the mechanical transfers were performed). The dark blue and magenta arrows from the Γ point to the K point of WS₂ indicate a 0° and 30° crystal orientation, respectively. The light-gray and cyan arrows from the K point of WS₂ to the K point of graphene illustrate phonon-assisted charge-transfer possibilities. (b) A graphical interpretation of the basic band structures of WS₂ and graphene shows that as one rotates the WS₂ Brillouin zone from 0° to 30° [magenta angular arc in (a)], the relative momentum difference between the K points of the two materials increases, represented by the color cyan. When the rotation is reversed, the K points of the two materials return to a relative momentum difference minimum, shown as a light-gray dotted line and a corresponding light-gray arrow, signifying the necessity for phonon assistance should charge transfer occur.

Raman shift of 355 cm⁻¹ and 417 cm⁻¹ [78], and excitons have an approximate radius in k space of about 0.15 \AA^{-1} [27], it is reasonable to expect some phonon-assisted charge

transfer in these systems. Further analysis on the Raman and PL spectra corresponding to changes in the dielectric environment and reflectance is included in the Supplemental Material [60,79–84].

Recent pump-probe measurements of the WS₂/graphene system provide an upper bound for the charge-transfer process of 350 fs, limited by the experimental time resolution [59]. Based on ARPES measurements and assuming that both materials' Brillouin zones are at a zero-degree orientation with respect to one another, 1.4 eV and 0.9 eV would be required for an electron or a hole, respectively, to initiate a charge-transfer process without phonon assistance [59]. When comparing our results to the bounds determined by other experimental methods, we find that they agree, thereby adding support to the conclusion that charge-transfer processes contribute to the observed exciton broadening.

V. CONCLUSIONS

In conclusion, by analyzing the reflectance contrast of bare WS₂ with that of various WS₂/graphene heterostructures, we are able to identify a 5–10-meV broadening in the exciton transitions of WS₂ induced by the presence of graphene. Both charge transfer and energy transfer were identified as the primary phenomena contributing to this broadening. Within experimental uncertainty, the broadening was found to have negligible dependence on the graphene thickness. The extracted values of 65–130 fs are a lower bound of the time scales of both energy- and charge-transfer processes.

ACKNOWLEDGMENTS

This work was made possible by the Center for Redefining Photovoltaic Efficiency through Molecule Scale Control, an Energy Frontier Research Center funded by the US Department of Energy, Office of Basic Energy Sciences, under Grant No. DE-SC0001085. Additional support was provided by the National Science Foundation through Grant No. DMR-1122594. H.M.H. and A.F.R. were supported by the NSF through an IGERT Fellowship under Grant No. DGE-1069240 and through a Graduate Research Fellowship, respectively. C.R. acknowledges support from the Keck Foundation and A.C. from the Alexander von Humboldt Foundation through a Feodor Lynen Research Fellowship and from the Deutsche Forschungsgemeinschaft through the Emmy Noether Programme (CH 1672/1-1). We would like to thank Arend van der Zande and Fan Zhang for fruitful discussions.

- [1] K. S. Novoselov, A. K. Geim, S. V. Morozov, D. Jiang, Y. Zhang, S. V. Dubonos, I. V. Grigorieva, and A. A. Firsov, *Science* **306**, 666 (2004).
- [2] A. K. Geim and K. S. Novoselov, *Nat. Mater.* **6**, 183 (2007).
- [3] A. K. Geim, *Science* **324**, 1530 (2009).
- [4] M. Bernardi, M. Palummo, and J. C. Grossman, *Nano Lett.* **13**, 3664 (2013).
- [5] K. S. Novoselov, D. Jiang, F. Schedin, T. J. Booth, V. V. Khotkevich, S. V. Morozov, and A. K. Geim, *Proc. Natl. Acad. Sci. U.S.A.* **102**, 10451 (2005).
- [6] K. F. Mak, C. Lee, J. Hone, J. Shan, and T. F. Heinz, *Phys. Rev. Lett.* **105**, 136805 (2010).
- [7] A. Splendiani, L. Sun, Y. Zhang, T. Li, J. Kim, C. Chim, G. Galli, and F. Wang, *Nano Lett.* **10**, 1271 (2010).
- [8] W. Zhao, Z. Ghorannevis, L. Chu, M. Toh, C. Kloc, P. Tan, and G. Eda, *ACS Nano* **7**, 791 (2013).
- [9] C. Ruppert, O. B. Aslan, and T. F. Heinz, *Nano Lett.* **14**, 6231 (2014).
- [10] G. Eda, H. Yamaguchi, D. Voiry, T. Fujita, M. Chen, and M. Chhowalla, *Nano Lett.* **11**, 5111 (2011).

- [11] L. Britnell, R. Ribeiro, A. Eckmann, R. Jalil, B. Belle, A. Mishchenko, Y.-J. Kim, R. Gorbachev, T. Georgiou, S. Morozov *et al.*, *Science* **340**, 1311 (2013).
- [12] C.-C. Shen, Y.-T. Hsu, L.-J. Li, and H.-L. Liu, *Appl. Phys. Express* **6**, 125801 (2013).
- [13] Y. Li, A. Chernikov, X. Zhang, A. Rigosi, H. M. Hill, A. M. van der Zande, D. A. Chenet, E.-M. Shih, J. Hone, and T. F. Heinz, *Phys. Rev. B* **90**, 205422 (2014).
- [14] N. Scheuschner, O. Ochedowski, A.-M. Kaulitz, R. Gillen, M. Schleberger, and J. Maultzsch, *Phys. Rev. B* **89**, 125406 (2014).
- [15] C. Yim, M. O'Brien, N. McEvoy, S. Winters, I. Mirza, J. G. Lunney, and G. S. Duesberg, *Appl. Phys. Lett.* **104**, 103114 (2014).
- [16] T. Cao, G. Wang, W. Han, H. Ye, C. Zhu, J. Shi, Q. Niu, P. Tan, E. Wang, B. Liu, and J. Feng, *Nat. Commun.* **3**, 887 (2012).
- [17] K. F. Mak, K. He, J. Shan, and T. F. Heinz, *Nat. Nanotechnol.* **7**, 494 (2012).
- [18] G. Sallen, L. Bouet, X. Marie, G. Wang, C. R. Zhu, W. P. Han, Y. Lu, P. H. Tan, T. Amand, B. L. Liu, and B. Urbaszek, *Phys. Rev. B* **86**, 081301 (2012).
- [19] H. Zeng, J. Dai, W. Yao, D. Xiao, and X. Cui, *Nat. Nanotechnol.* **7**, 490 (2012).
- [20] D. Xiao, G.-B. Liu, W. Feng, X. Xu, and W. Yao, *Phys. Rev. Lett.* **108**, 196802 (2012).
- [21] A. M. Jones, H. Yu, N. J. Ghimire, S. Wu, G. Aivazian, J. S. Ross, B. Zhao, J. Yan, D. G. Mandrus, D. Xiao, W. Yao, and X. Xu, *Nat. Nanotechnol.* **8**, 634 (2013).
- [22] D. Lagarde, L. Bouet, X. Marie, C. R. Zhu, B. L. Liu, T. Amand, P. H. Tan, and B. Urbaszek, *Phys. Rev. Lett.* **112**, 047401 (2014).
- [23] K. F. Mak, K. L. McGill, J. Park, and P. L. McEuen, *Science* **344**, 1489 (2014).
- [24] G. Wang, L. Bouet, D. Lagarde, M. Vidal, A. Balocchi, T. Amand, X. Marie, and B. Urbaszek, *Phys. Rev. B* **90**, 075413 (2014).
- [25] X. Xu, W. Yao, D. Xiao, and T. F. Heinz, *Nat. Phys.* **10**, 343 (2014).
- [26] K. He, N. Kumar, L. Zhao, Z. Wang, K. F. Mak, H. Zhao, and J. Shan, *Phys. Rev. Lett.* **113**, 026803 (2014).
- [27] A. Chernikov, T. C. Berkelbach, H. M. Hill, A. Rigosi, Y. Li, O. B. Aslan, D. R. Reichman, M. S. Hybertsen, and T. F. Heinz, *Phys. Rev. Lett.* **113**, 076802 (2014).
- [28] M. M. Ugeda, A. J. Bradley, S.-F. Shi, F. H. da Jornada, Y. Zhang, D. Y. Qiu, S.-K. Mo, Z. Hussain, Z.-X. Shen, F. Wang *et al.*, *Nat. Mater.* **13**, 1091 (2014).
- [29] Z. Ye, T. Cao, K. O'Brien, H. Zhu, X. Yin, Y. Wang, S. G. Louie, and X. Zhang, *Nature (London)* **513**, 214 (2014).
- [30] G. Wang, X. Marie, I. Gerber, T. Amand, D. Lagarde, L. Bouet, M. Vidal, A. Balocchi, and B. Urbaszek, *Phys. Rev. Lett.* **114**, 097403 (2015).
- [31] C. Zhang, A. Johnson, C. L. Hsu, L. J. Li, and C. K. Shih, *Nano Lett.* **14**, 2443 (2014).
- [32] A. R. Klots, A. K. M. Newaz, B. Wang, D. Prasai, H. Krzyzanowska, D. Caudel, N. J. Ghimire, J. Yan, B. L. Ivanov, K. A. Velizhanin *et al.*, *Sci. Rep.* **4**, 6608 (2014).
- [33] H. M. Hill, A. F. Rigosi, C. Roquelet, A. Chernikov, T. C. Berkelbach, D. R. Reichman, M. S. Hybertsen, L. E. Brus, and T. F. Heinz, *Nano Lett.* **15**, 2992 (2015).
- [34] K. F. Mak, K. He, C. Lee, G. H. Lee, J. Hone, T. F. Heinz, and J. Shan, *Nat. Mater.* **12**, 207 (2013).
- [35] J. S. Ross, S. Wu, H. Yu, N. J. Ghimire, A. M. Jones, G. Aivazian, J. Yan, D. G. Mandrus, D. Xiao, W. Yao, and X. Xu, *Nat. Commun.* **4**, 1474 (2013).
- [36] W. Jin, P.-C. Yeh, N. Zaki, D. Chenet, G. Arefe, Y. Hao, A. Sala, T. O. Montes, J. I. Dadap, A. Locatelli, J. Hone, and R. M. Osgood, Jr., *Phys. Rev. B* **92**, 201409 (2015).
- [37] D. Jariwala, V. K. Sangwan, L. J. Lauhon, T. J. Marks, and M. C. Hersam, *ACS Nano* **8**, 1102 (2014).
- [38] K. Roy, M. Padmanabhan, S. Goswami, T. P. Sai, G. Ramalingam, S. Raghavan, and A. Ghosh, *Nat. Nanotechnol.* **8**, 826 (2013).
- [39] W. J. Yu, Z. Li, H. Zhou, Y. Chen, Y. Wang, Y. Huang, and X. Duan, *Nat. Mater.* **12**, 246 (2012).
- [40] M.-H. Chiu, C. Zhang, H. W. Shiu, C.-P. Chu, C.-H. Chen, C.-Y. S. Chang, C.-H. Chen, M.-Y. Chou *et al.*, *Nat. Commun.* **6**, 7666 (2015).
- [41] Y. Yu, S. Hu, L. Su, L. Huang, Y. Liu, Z. Jin, A. A. Purezky, D. B. Geohegan, K. W. Kim, and Y. Zhang, *Nano Lett.* **15**, 486 (2015).
- [42] X. Hong, J. Kim, S. F. Shi, Y. Zhang, C. Jin, Y. Sun, S. Tongay, J. Wu, Y. Zhang, and F. Wang, *Nat. Nanotechnol.* **9**, 682 (2014).
- [43] P. Rivera, J. R. Schaibley, A. M. Jones, J. S. Ross, S. Wu, G. Aivazian, P. Klement, N. J. Ghimire, J. Yan, and D. G. Mandrus, *Nat. Commun.* **6**, 6242 (2015).
- [44] H. Fang, C. Battaglia, C. Carraro, S. Nemsak, B. Ozdol, J. S. Kang, H. A. Bechtel, S. B. Desai, F. Kronast, A. A. Unal *et al.*, *Proc. Natl. Acad. Sci. U.S.A.* **111**, 6198 (2014).
- [45] Y. Gong, J. Lin, X. Wang, G. Shi, S. Lei, Z. Lin, X. Zou, G. Ye, R. Vajtai, B. Yakobson, H. Terrones, M. Terrones, B. K. Tay, J. Lou, S. T. Pantelides, Z. Liu, W. Zhou, and P. M. Ajayan, *Nat. Mater.* **13**, 1135 (2014).
- [46] M.-H. Chiu, M.-Y. Li, W. Zhang, W.-T. Hsu, W.-H. Chang, M. Terrones, H. Terrones, and L.-J. Li, *ACS Nano* **8**, 9649 (2014).
- [47] K. Liu, Q. Yan, M. Chen, W. Fan, Y. Sun, J. Suh, D. Fu, S. Lee, J. Zhou, S. Tongay, J. Ji, J. B. Neaton, and J. Wu, *Nano Lett.* **14**, 5097 (2014).
- [48] S. Tongay, W. Fan, J. Kang, J. Park, U. Koldemir, J. Suh, D. S. Narang, K. Liu, J. Ji, J. Li, R. Sinclair, and J. Wu, *Nano Lett.* **14**, 3185 (2014).
- [49] G. W. Shim, K. Yoo, S. B. Seo, J. Shin, D. Y. Jung, I. S. Kang, C. W. Ahn, B. J. Cho, and S. Y. Choi, *ACS Nano* **8**, 6655 (2014).
- [50] F. Ceballos, M. Z. Bellus, H. Chiu, and H. Zhao, *ACS Nano* **8**, 12717 (2014).
- [51] A. F. Rigosi, H. M. Hill, Y. Li, A. Chernikov, and T. F. Heinz, *Nano Lett.* **15**, 5033 (2015).
- [52] F. Ceballos, M.-G. Ju, S. D. Lane, X. C. Zeng, and H. Zhao, *Nano Lett.* **17**, 1623 (2017).
- [53] O. A. Ajayi, J. V. Ardelean, G. D. Shepard, J. Wang, A. Antony, T. Taniguchi, K. Watanabe, T. F. Heinz, S. Strauf, X.-Y. Zhu, and J. C. Hone, *2D Mater.* **4**, 031011 (2017).
- [54] C. Lan, C. Li, S. Wang, T. He, Z. Zhou, D. Wei, H. Guo, H. Yang, and Y. Liu, *J. Mater. Chem. C* **5**, 1494 (2017).
- [55] J. He, N. Kumar, M. Z. Bellus, H.-Y. Chiu, D. He, Y. Wang, and H. Zhao, *Nat. Commun.* **5**, 5622 (2014).
- [56] T. Georgiou, R. Jalil, B. D. Belle, L. Britnell, R. V. Gorbachev, S. V. Morozov, Y.-J. Kim, A. Gholinia, S. J. Haigh, O. Makarovskiy *et al.*, *Nat. Nanotechnol.* **8**, 100 (2013).
- [57] F. H. L. Koppens, T. Mueller, P. Avouris, A. C. Ferrari, M. S. Vitiello, and M. Polini, *Nat. Nanotechnol.* **9**, 780 (2014).

- [58] A. Raja, A. Chaves, J. Yu, G. Arefe, H. M. Hill, A. F. Rigosi, T. C. Berkelbach, P. Nagler, C. Schuller, T. Korn, C. Nuckolls, J. Hone, L. E. Brus, T. F. Heinz, D. R. Reichman, and A. Chernikov, *Nat. Commun.* **8**, 15251 (2017).
- [59] J. He, D. He, Y. Wang, and H. Zhao, *Opt. Express* **25**, 1949 (2017).
- [60] See Supplemental Material at <http://link.aps.org/supplemental/10.1103/PhysRevB.96.205401> for more information about the observed broadening, exciton peak redshifts, PL quenching, Raman spectroscopy of graphene, spatial and processing variation, and interface quality.
- [61] H. Zhu, J. Wang, Z. Gong, Y. D. Kim, J. Hone, and X.-X. Zhu, *Nano Lett.* **17**, 3591 (2017).
- [62] T. Korn, S. Heydrich, M. Hirmer, J. Schmutzler, and C. Schüller, *Appl. Phys. Lett.* **99**, 102109 (2011).
- [63] M. Selig, G. Berghäuser, A. Raja, P. Nagler, C. Schüller, T. F. Heinz, T. Korn, A. Chernikov, E. Malic, and A. Knorr, *Nat. Commun.* **7**, 13279 (2016).
- [64] A. Chernikov, A. M. van der Zande, H. M. Hill, A. F. Rigosi, A. Velauthapillai, J. Hone, and T. F. Heinz, *Phys. Rev. Lett.* **115**, 126802 (2015).
- [65] W. Jin, P.-C. Yeh, N. Zaki, D. Zhang, J. T. Sadowski, A. Al-Mahboob, A. M. van Der Zande, D. A. Chenet, J. I. Dadap, I. P. Herman, P. Sutter, J. Hone, and R. M. Osgood, Jr., *Phys. Rev. Lett.* **111**, 106801 (2013).
- [66] S. Ulstrup, J. Katoch, R. J. Koch, D. Schwarz, S. Singh, K. M. McCreary, H. K. Yoo, J. Xu, B. T. Jonker, R. K. Kawakami, A. Bostwick, E. Rotenberg, and C. Jozwiak, *ACS Nano* **10**, 10058 (2016).
- [67] S. Ulstrup, A. G. Čabo, J. A. Miwa, J. M. Riley, S. S. Grønberg, J. C. Johannsen, C. Cacho, O. Alexander, R. T. Chapman, E. Springate, M. Bianchi, M. Dendzik, J. V. Lauritsen, P. D. C. King, and P. Hofmann, *ACS Nano* **10**, 6315 (2016).
- [68] N. R. Wilson, P. V. Nguyen, K. Seyler, P. Rivera, A. J. Marsden, Z. P. L. Laker, G. C. Constantinescu, V. Kandyba, A. Barinov, N. D. M. Hine, X. Xu, and D. H. Cobden, *Sci. Adv.* **3**, e1601832 (2017).
- [69] A. Raja, A. Montoya-Castillo, J. Zultak, X.-X. Zhang, Z. Ye, C. Roquelet, D. A. Chenet, A. M. van der Zande, P. Huang, S. Jockusch, J. Hone, D. R. Reichman, L. E. Brus, and T. F. Heinz, *Nano Lett.* **16**, 2328 (2016).
- [70] Z. Chen, S. Berciaud, C. Nuckolls, T. F. Heinz, and L. E. Brus, *ACS Nano* **4**, 2964 (2010).
- [71] F. Prins, A. J. Goodman, and W. A. Tisdale, *Nano Lett.* **14**, 6087 (2014).
- [72] F. Federspiel, G. Froehlicher, M. Nasilowski, S. Pedetti, A. Mahmood, B. Doudin, S. Park, J.-O. Lee, D. Halley, B. Dubertret, P. Gilliot, and S. Berciaud, *Nano Lett.* **15**, 1252 (2015).
- [73] P. L. Hernández-Martínez, A. O. Govorov, and H. V. Demir, *J. Phys. Chem. C* **118**, 4951 (2014).
- [74] L. Gaudreau, K. J. Tielrooij, G. E. D. K. Prawiroatmodjo, J. Osmond, F. J. G. de Abajo, and F. H. L. Koppens, *Nano Lett.* **13**, 2030 (2013).
- [75] A. Naeem, F. Masia, S. Christodoulou, I. Moreels, P. Borri, and W. Langbein, *Phys. Rev. B* **91**, 121302 (2015).
- [76] W. Wurth and D. Menzel, *Chem. Phys.* **251**, 141 (2000).
- [77] J. Gudde and U. Hofer, *Prog. Surf. Sci.* **80**, 49 (2005).
- [78] A. Berkdemir, H. R. Gutiérrez, A. R. Botello-Méndez, N. Perea López, A. L. Elías, C.-I. Chia, B. Wang, V. H. Crespi, F. López-Urías, and J.-C. Charlier, *Sci. Rep.* **3**, 1755 (2013).
- [79] D. Sun, Y. Rao, G. A. Reider, G. Chen, Y. You, L. Brezin, A. R. Harutyunyan, and T. F. Heinz, *Nano Lett.* **14**, 5625 (2014).
- [80] L. Wang, Z. Chen, C. Dean, T. Tanigushi, K. Watanabe, L. E. Brus, and J. Hone, *ACS Nano* **6**, 9314 (2012).
- [81] A. C. Ferrari, J. C. Meyer, V. Scardaci, C. Casiraghi, M. Lazzeri, F. Mauri, S. Piscanec, D. Jiang, K. S. Novoselov, S. Roth, and A. K. Geim, *Phys. Rev. Lett.* **97**, 187401 (2006).
- [82] J. Yan, Y. Zhang, P. Kim, and A. Pinczuk, *Phys. Rev. Lett.* **98**, 166802 (2007).
- [83] M. Bruna, A. K. Ott, M. Ijäs, D. Yoon, U. Sassi, and A. C. Ferrari, *ACS Nano* **8**, 7432 (2014).
- [84] A. Das, S. Pisana, B. Chakraborty, S. Piscanec, S. K. Saha, U. V. Waghmare, K. S. Novoselov, H. R. Krishnamurthy, A. K. Geim, A. C. Ferrari, and A. K. Sood, *Nat. Nanotechnol.* **3**, 210 (2008).